



**Correlating Nanoscale Secondary Ion Mass Spectrometry  
and Atom Probe Tomography Analysis of Uranium  
Enrichment in Metallic Nuclear Fuel**

Journal:	<i>Analyst</i>
Manuscript ID	AN-COM-09-2020-001831.R1
Article Type:	Communication
Date Submitted by the Author:	23-Oct-2020
Complete List of Authors:	Kautz, Elizabeth; Pacific Northwest National Laboratory, National Security Directorate Cliff, John; PNNL, EED Lach, Timothy; Oak Ridge National Laboratory Reilly, Dallas; Pacific Northwest National Laboratory, National Security Directorate Devaraj, Arun; Pacific Northwest National Lab, Environmental Molecular Sciences lab

## COMMUNICATION

# Correlating Nanoscale Secondary Ion Mass Spectrometry and Atom Probe Tomography Analysis of Uranium Enrichment in Metallic Nuclear Fuel

Received 00th January 20xx,  
Accepted 00th January 20xx

Elizabeth Kautz,<sup>a</sup> John Cliff,<sup>b</sup> Timothy Lach,<sup>c+</sup> Dallas Reilly,<sup>a</sup> and Arun Devaraj<sup>d\*‡</sup>

DOI: 10.1039/x0xx00000x

**Accurate measurements of <sup>235</sup>U enrichment within metallic nuclear fuels are essential to understanding material performance in a neutron irradiation environment, and the origin of secondary phases (e.g. uranium carbides). In this work, we analyse <sup>235</sup>U enrichment in matrix and carbide phases in low enriched uranium alloyed with 10 wt. % Mo via two chemical imaging modalities—nanoscale secondary ion mass spectrometry (NanoSIMS) and atom probe tomography (APT). Results from NanoSIMS and APT are compared to understand accuracy and utility of both approaches across length scales. NanoSIMS and APT provide consistent results, with no statistically significant difference between nominal enrichment (19.95 ± 0.14 at. % <sup>235</sup>U) and that measured for metal matrix and carbide inclusions.**

## Introduction

Quantifying U enrichment, defined here as the percentage of <sup>235</sup>U atoms relative to atoms of all U isotopes, is critical for several applications, including nuclear fuel processing,<sup>1–3</sup> Safeguards, and forensics.<sup>4–7</sup> U enrichment provides valuable insight into material age, origin, and processing history. In

nuclear forensics studies, for example, precise measurement of U enrichment is used to investigate illicit trafficking, and to evaluate nuclear fuel processing history. For the production of nuclear fuels, U enrichment and isotopic homogeneity have important consequences for neutronics, heat distribution, and fuel life cycle. Currently, there is a global effort to convert research and medical isotope reactors from highly enriched U (HEU) to low enriched U (LEU, defined as greater than 0.7 and less than 20 wt. % <sup>235</sup>U) fuel to reduce proliferation risks.<sup>8</sup> Traditionally, these reactors utilize HEU UO<sub>2</sub> to achieve reactor performance requirements, however, metallic fuel in a monolithic plate type design can meet similar performance and design constraints.

A candidate for the replacement of traditional HEU fuels is LEU alloyed with 10 wt. % molybdenum (U-10Mo). The 10 wt. % Mo alloying addition is selected to retain the γ-U body centred cubic (BCC) phase at temperatures below 565 °C, which has desirable swelling characteristics in a neutron irradiation environment.<sup>9</sup> To meet the less than 20 wt. % <sup>235</sup>U enrichment (and thus be considered as a LEU fuel), HEU metal is inductively melted with either depleted (DU, ~0.2 wt. % <sup>235</sup>U) and/or natural U (NU, ~0.7 wt. % <sup>235</sup>U) metal in a process referred to as ‘down-blending’.<sup>10</sup> Homogenous distribution of <sup>235</sup>U in U-10Mo is required to ensure uniform fission rate and fission density in the fuel during reactor operation due to their impacts on dimensional stability and fuel robustness.<sup>11</sup> Homogeneity of <sup>235</sup>U can also affect distribution and rate of fission product formation, and resultant degradation of material properties (e.g. thermal conductivity, mechanical strength, etc.).<sup>12</sup> However, the kinetics of down blending are slow, leading to possible heterogeneity in <sup>235</sup>U distribution.<sup>13</sup> The length scales over which <sup>235</sup>U is homogeneously distributed has recently been studied in U oxides,<sup>5, 7</sup> however, <sup>235</sup>U homogeneity remains largely unexplored in fabricated metallic fuels, despite being critical to fuel performance and qualification.

In fuel plates, U isotopes are distributed in both matrix and secondary phases.<sup>3, 14</sup> Non-metallic secondary inclusions such as uranium carbides (UC) are often present, and may be

<sup>1</sup>National Security Directorate, Pacific Northwest National Laboratory, 902 Battelle Boulevard, Richland, WA 99354

<sup>2</sup>Earth and Biological Sciences Directorate, Pacific Northwest National Laboratory, Richland, WA

<sup>3</sup>Energy and Environment Directorate, Pacific Northwest National Laboratory, Richland, WA

<sup>4</sup>Physical and Computational Sciences Directorate, Pacific Northwest National Laboratory, Richland, WA

<sup>+</sup>currently at Oak Ridge National Laboratory, 1 Bethel Valley Road, Oak Ridge, TN 37830

\*corresponding author: arun.devaraj@pnnl.gov

‡ This manuscript has been authored in part by UT-Battelle, LLC, under contract DE-AC05-00OR22725 with the US Department of Energy (DOE). The US government retains and the publisher, by accepting the article for publication, acknowledges that the US government retains a nonexclusive, paid-up, irrevocable, worldwide license to publish or reproduce the published form of this manuscript, or allow others to do so, for US government purposes. DOE will provide public access to these results of federally sponsored research in accordance with the DOE Public Access Plan (<http://energy.gov/downloads/doe-public-access-plan>).

DOI: 10.1039/x0xx00000x

retained from feedstock materials or formed during the casting process. If these inclusions (typically nanometres to micrometres in diameter) deviate from the nominal 20%  $^{235}\text{U}$ , heterogeneities in fission product generation and temperature may exist within the fuel during reactor operation. Such heterogeneities therefore have implications for safe and reliable performance throughout the fuel's lifecycle.

Mapping isotopic content of non-metallic inclusions can be used to determine the spatial distribution of  $^{235}\text{U}$ , and can help improve predictive capabilities of fuel performance in an operating reactor. While APT is a valuable technique for identifying elemental and isotopic composition of materials in nanoscopic volumes with high spatial and mass resolving power, mapping larger inclusions is not practical. Recently, the distribution of U isotopes has been explored in nuclear materials at length scales ranging from nanometres (nm) to micrometres ( $\mu\text{m}$ ),<sup>3, 5, 7, 15</sup> however, to date, no works have correlated results across nanometre to micrometre length scales using different modalities.

Several methods are commonly used to measure isotopic composition, including radiometric counting, optical spectroscopy,<sup>16</sup> and mass spectrometry techniques.<sup>17</sup> Mass spectrometry techniques such as thermal ionization mass spectrometry (TIMS),<sup>18</sup> SIMS,<sup>19</sup> and inductively coupled plasma mass spectrometry ICP-MS are commonly used.<sup>20</sup> Other approaches including quadrupole time of flight mass spectrometry<sup>21</sup>, the combination of laser ablation (LA)-ICP-MS and LA-optical emission spectroscopy (LA-OES)<sup>22</sup>, and the fusion of SIMS and energy dispersive spectroscopy (EDS)<sup>23</sup> imaging have also been explored. APT has recently been shown to be highly valuable for analysing enrichment and isotopic abundances in nuclear materials.<sup>3, 4, 15</sup> One method that could provide complementary information is nanoscale secondary ion mass spectrometry (NanoSIMS), which has high lateral spatial resolution ( $< 1 \mu\text{m}$ ), and has been used extensively for spatially resolved isotopic analyses.<sup>5, 24, 25</sup> In this study, we map U enrichment in UC and the surrounding  $\gamma$ -UMo matrix via the complementary modalities of NanoSIMS and APT. A U-10Mo fuel foil with a nominal enrichment of  $19.75 \pm 0.14 \text{ wt. \%}$  ( $19.95 \pm 0.14 \text{ at. \%}$ )<sup>26</sup> was analysed and U enrichment in both phases, measured by both techniques, was compared. These measurements allow for a direct comparison of U enrichment across length scales and resolutions. This work has implications for nuclear forensics, geochronology, and environmental remediation, where multi-length-scale, comparative analyses of isotopic compositions may be advantageous.

## Experimental Materials and Methods

The fuel plate examined in this work was fabricated at the Y-12 National Security Complex and consisted of a U-10Mo fuel foil with a Zr inter-diffusion barrier layer on each side and clad in Al alloy 6061. The U-10Mo fuel was manufactured by melting and casting HEU, DU, and Mo with appropriate proportions to obtain the desired 10 wt% Mo and  $^{235}\text{U}$  enrichment ( $\sim 19.75 \text{ wt. \%}$ ). The U-10Mo casting was then cut and formed into foils via thermomechanical processing<sup>2</sup> and the Zr interlayer was

bonded to the fuel foil via hot isostatic pressing.<sup>27</sup> The fuel plate was sectioned and prepared via standard metallographic polishing procedures for analysis.<sup>28</sup>

Samples were prepared for APT and NanoSIMS by following a standard focused ion beam/scanning electron microscope (FIB/SEM) preparation procedure for a TEM lamella, where sample thickness was kept at  $\sim 1\text{-}3 \mu\text{m}$ . Each sample contained both the U-10Mo matrix and multiple UC inclusions. Site-specific FIB lift-outs<sup>29, 30</sup> were performed to allow for targeted analysis of the UC/ $\gamma$ -UMo interface and constituent phases via APT and lamellae were mounted onto a Si wafer for subsequent NanoSIMS analysis.

NanoSIMS analyses were performed using a Cameca NanoSIMS 50L. A detailed description of analysis methods has been described previously.<sup>24</sup> Briefly, a 16 keV  $\text{O}^+$  beam was used to pre-sputter the samples prior to isotope image collection. Secondary positive ions were accelerated to 8 keV and counted using electron multipliers (EM). Image dimensions were set so that the entire lamellae was captured using a  $256 \times 256$  pixel array ( $\sim 35 \mu\text{m} \times 35 \mu\text{m}$ ). Isotopes of interest ( $^{235}\text{U}^+$  and  $^{238}\text{U}^+$ ) were detected sequentially on different EMs using magnetic peak switching. Images were processed using the Fiji distribution of the ImageJ plugin OpenMIMS [<https://nano.bwh.harvard.edu/openmims>]. Pixel  $\times$  pixel deadtime corrections were performed and region of interest (ROI) intensity data were imported into an Excel spreadsheet for further data reduction and corrected for instrumental mass fractionation (IMF) assuming a linear mass fractionation scheme. A certified reference material (CRM U010) was analysed during the same session to calibrate for IMF. The IMF was calculated using image analyses of six-single CRM U010 particles. Propagated uncertainties included internal uncertainties based on Poisson counting statistics, the standard deviation (SD) of multiple IMF estimates derived from the reference particle analyses, and the uncertainty of the reported certified values from CRM U010.

A CAMECA LEAP 4000X HR system equipped with a 355 nm wavelength ultraviolet (UV) laser was used for all APT data collection. APT user-selected parameters for data collection in this work include 100 pJ laser energy, 100 kHz pulse frequency, 45 K specimen temperature, and 0.005 atoms/pulse detection rate. The analysis chamber pressure was kept at a less than  $2 \times 10^{-11}$  Torr. The overall detection efficiency of the LEAP used in this work is approximately 36%. APT data sets analysed and reported here ranged in size between  $\sim 1$  and 20 million ions, and either contained UC,  $\gamma$ -UMo, or both. All data sets were analysed using the Integrated Visualization and Analysis Software (IVAS), version 3.8.5, using manual ranging criteria detailed in the Supplementary Information (SI), Figure S3. For calculating U isotopic abundances, the ratios of  $^{235}\text{U}^{3+}$  and  $^{238}\text{U}^{3+}$  ions were used for the following reasons: (1)  $\text{U}^{3+}$  ions are the majority of U ion species collected via the APT technique; and (2) Use of the  $\text{U}^{3+}$  ions did not require peak deconvolution, thus simplifying the data analysis process and reducing error introduced into the analysis procedure. In our prior work, we found U enrichment calculated using isotopes in the  $\text{U}^{3+}$  charge state (versus  $\text{U}^{2+}$ )

resulted in more consistent, repeatable measurements between multiple APT specimens, and lower error.<sup>3</sup> Hence, we apply the same data analysis approach here.

## Results and Discussion

A representative scanning electron micrograph of the microstructure of a U-10Mo sample analysed in this work is presented in Figure 1. The secondary phase (i.e. inclusions) of interest, identified as UC in previous studies,<sup>3</sup> appear clustered and aligned along the longitudinal direction due to the multiple thermomechanical processing steps involved in fuel fabrication (e.g. hot and cold rolling).<sup>31</sup> Micrographs also illustrate two types of inclusions: coarse (~micrometres in diameter) and fine (~nanometres in diameter, aligned along grain boundaries). Here, we focus on the coarse inclusions, as fine-scale inclusions were analysed in prior work.<sup>3</sup>

From the fuel plate, three different FIB lift-outs were analysed via NanoSIMS, where each lift-out was taken from a different region of the plate. For each FIB lift-out sample, multiple regions of interest (ROIs) for isotopic analysis were selected from both the  $\gamma$ -UMo matrix and UC phases. It is noted here that specimen refers to the material sectioned from the bulk fuel foil via FIB milling, and ROI refers to a sub-region of the specimen ion image acquired via NanoSIMS. An example SEM image of a lift-out and representative signal intensity maps (where ROIs selected for isotopic image analysis are identified) is presented in Figure 2. Contrast observed in the intensity maps show that UC signal intensity was higher in comparison to the metallic matrix phase. Many UC inclusions were fractured during rolling and these smaller fragments were each selected as a ROI as shown in Figure 2(c).

To investigate the homogeneity of U enrichment at even finer length scales, nanoscale volumes from the same LEU-Mo fuel foil were analyzed via APT. Several needle specimens fabricated from different locations in the fuel foil were analysed (a similar approach as used in the selection of NanoSIMS samples). Mapping of U enrichment across interfaces was performed in addition to bulk isotopic analyses from needle specimens containing only a single phase. Mass spectra and element distribution maps obtained via APT analyses are provided in the SI, Figure S2. An example APT data set is given in Figure 3, and includes both UC and  $\gamma$ -UMo phases of interest. Figure 3(a) shows the 3D element distribution map and

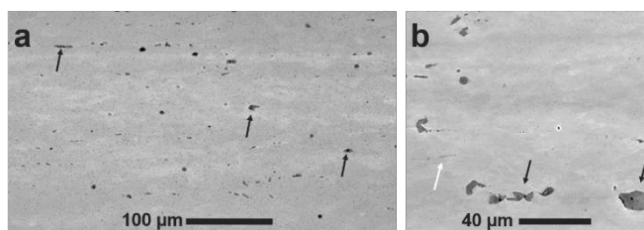


**Fig. 1.** Microstructure of fabricated LEU-10Mo fuel plate. Scanning electron microscope-backscattered electron (SEM-BSE) images of the LEU-10Mo fuel microstructure analysed via NanoSIMS and APT. Black arrows point toward UC inclusions on the order of micrometres, and the white arrow in (b) points towards nanoscale UC inclusions.

corresponding isotopic and compositional mapping across the  $\gamma$ -UMo/UC interface and are reported in Figure 3(b) and (c), respectively. The direction of data analysis corresponding to Figure 3(b,c) is indicated by the white arrow in Figure 3(a). The dashed red line in Figure 3(b) is the nominal enrichment value of 19.95%.

U enrichment of specimens analysed via NanoSIMS and APT are shown in Figure 4. Statistical analyses were performed on the data reported in Figure 4 and are summarized in Table 1. The Figure 4 box-and-whisker plots illustrate distribution, median and mean values, and variability, compared to the nominal value of 19.95 at. % <sup>235</sup>U, for both phases and measurement techniques. Individual data points are given next to each box-and-whisker plot, where each data point is from one NanoSIMS ROI, or one needle specimen in the case of APT. Individual data points are presented from a minimum of two FIB liftouts for both NanoSIMS and APT, sampled from different locations in the fuel plate. Specifically, for the UMo matrix, 14 ROIs were analysed via NanoSIMS, and 9 needle specimens/reconstructed volumes for APT. For UC, there were 14 ROIs from NanoSIMS analysis, and 3 volumes reconstruction from APT.

Both NanoSIMS and APT measurement modalities gave similar results for U enrichment measurements, however, there are distinct differences between the techniques that should be mentioned. For example, we used reference analyses to calibrate the U enrichment estimated by NanoSIMS ROI measurements. Although these measurements improved accuracy of the ROI analyses, they also increased overall uncertainty. In contrast, it is not standard practice to run reference samples prior to the analyte of interest for calibration of APT data as IMF for the technique is small. The total

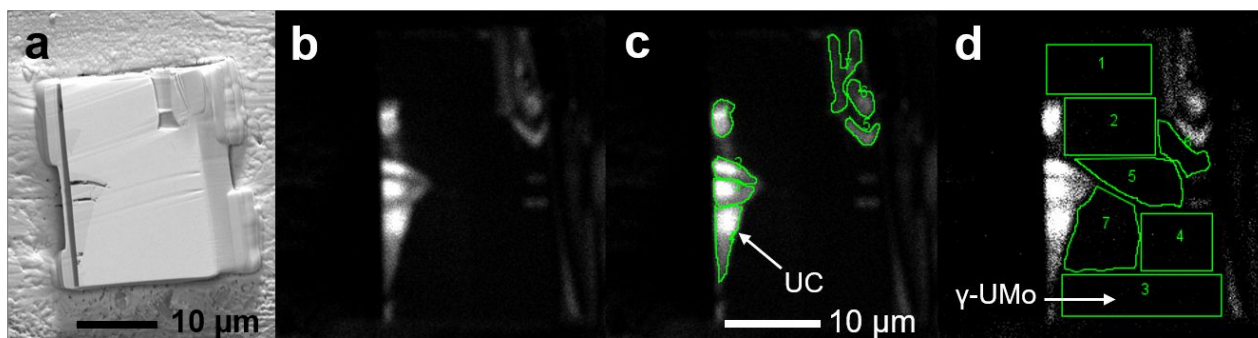


**Fig. 2.** Microstructural features analysed via NanoSIMS. (a) Secondary electron SEM image of the sample analysed, (b) corresponding <sup>238</sup>U<sup>+</sup> ion image, (c) ion image with UC phase ROIs outlined in green, and (d) the same ion image from (c) with the matrix regions analysed outlined in green. Grayscale shows relative signal intensity.

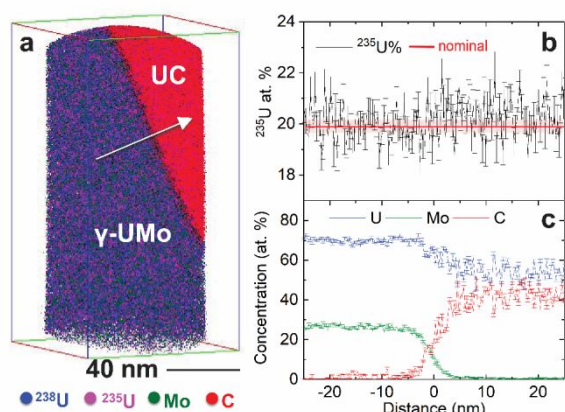


**Figure 3.** Composition and isotopic analysis across a UC/UMo matrix interface analyzed via APT. (a) 3D element distribution, where the arrow indicates direction of data analysis, (b)  $^{235}\text{U}$  enrichment across this same interface, and (c) elemental composition across the interface, including U, Mo, and C in at. %. In (b) nominal enrichment of  $19.95 \pm 0.014$  at. %  $^{235}\text{U}$  is indicated by the solid red line at 19.95 at. %, and the shaded red box shows  $\pm 1$  standard deviation (19.81 – 20.09 at. %).

number of ions in APT data sets varied from  $\sim 165,000$  to  $\sim 20,000,000$ . Additional details on APT data set size and factors in the data analysis process impacting enrichment calculations (e.g. ranging criteria) are provided in the SI, Appendices 2-3. NanoSIMS was also used to map larger volumes than APT, potentially increasing the range of intrasample enrichment estimates. To rigorously compare U enrichment estimates between data sets collected using the different measurement modalities, statistical analyses of the data were performed.

Student's t-tests for each set of NanoSIMS and APT data for the UMo matrix and UC phases were performed to test the null hypothesis that the mean U enrichments ( $^{235}\text{U}$ ) (i.e. NanoSIMS UMo, APT UMo, NanoSIMS UC, APT UC) were not equal to 19.95 at. %. Analyses were performed for each data set and we found that the p-value is greater than  $\alpha$  at the 0.05 significance level, hence there was no statistically significant difference between the mean of each data set and the 19.95 at. % U enrichment specification. It is noted here, that Table 1 reports lower and upper limits of a 95% confidence interval (CI), for reference. From statistical analysis, we find mean enrichment values estimated using both measurement modalities are in good agreement with the LEU specification for each phase studied here.

An important consideration in the development of nuclear fuels, is the definition of LEU versus HEU. LEU is defined by the Nuclear Regulatory Commission (NRC) as  $0.72\% < \text{LEU} < 20\%$   $^{235}\text{U}$ , where any material with higher enrichment is treated as HEU. Thus, precise measurement of enrichment is important to evaluate the development and continued manufacture of new nuclear fuels. Based on our measurements,  $^{235}\text{U}$  composition in the analysed fuel foil is approximately 20%  $^{235}\text{U}$ . Since no DU or HEU enrichment levels were found in the volumes analysed, this result suggests that the  $^{235}\text{U}$  is consistent with expected for the LEU fuel from nano to micron length scales within the volumes analysed; no heterogeneities in  $^{235}\text{U}$  distribution were observed in either APT or NanoSIMS analyses. Additionally, the UC

inclusions analysed all had enrichment values close to the LEU specification, and thus we conclude were formed during fuel processing and not retained from DU or HEU feedstocks. We suggest that spatially resolved U isotopic enrichment results such as those presented here can be correlated with the results of post-irradiation examination of these fuels and fission products for the purpose of understanding changes in spatial distribution of U isotopes as a function of burn-up.

While NanoSIMS and APT analyses yielded consistent enrichment results, the techniques provide complementary information. NanoSIMS allows for analysis of much larger microstructural features in a single image, whereas the volume represented in APT data sets is much smaller. However, if there are nanoscale precipitates on the order of a few nm or tens of

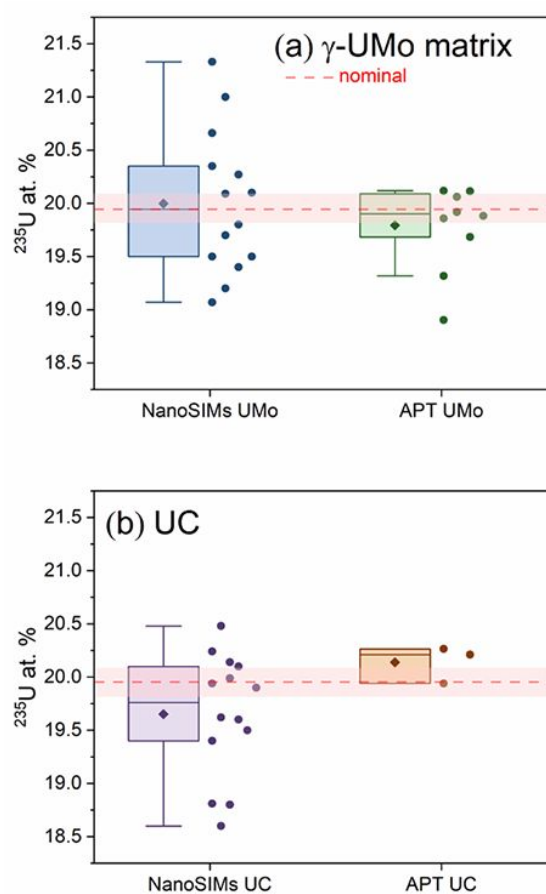


**Fig. 4.** Summary of U enrichment measured via NanoSIMS and APT for: (a) UMo matrix, and (b) UC phases in a LEU-10Mo fuel. Nominal enrichment of  $19.95 \pm 0.14$  at. %  $^{235}\text{U}$  is indicated by the dashed red line at 19.95 at. % and the shaded red box showing  $\pm 1$  standard deviation (19.81 – 20.09 at. %  $^{235}\text{U}$ ). Box and whisker plots are given for all NanoSIMS and APT data collected for each phase. In each box and whisker plot, the median is shown as a horizontal line, the mean value as a diamond, and 25<sup>th</sup> to 75<sup>th</sup> percentiles (i.e., interquartile range, or IQR) of the data are given by the box. The whiskers indicate  $\pm 1.5$  IQR. Each point next to each box and whisker plot represents one individual data point (ROI for NanoSIMS, or reconstructed dataset for APT).

nm in diameter, or grain boundaries, APT can effectively analyse their elemental and isotopic composition, which may be more difficult in larger area mapping using NanoSIMS. Recently, an APT study of  $\text{U}_3\text{O}_8$  reference materials reported isotopic measurements within  $\pm 1.5\%$  relative error to reference values,

where accuracy and repeatability of measurements were limited by the number of U atoms collected during analysis.<sup>32</sup> LA-ICP-MS has also recently been demonstrated for mapping U enrichment, although at a much larger length scale (i.e. 5  $\mu\text{m}$  distance between spots in a 50  $\mu\text{m}$  by 100  $\mu\text{m}$  array).<sup>7, 24</sup> Though mapping enrichment via LA-ICP-MS is rapid and has higher throughput compared to the techniques used here, the nanometre- to micrometre-scale carbide inclusions

encountered in the metallic fuel plate studied must be analysed using higher resolution tools. Hence, the combination of NanoSIMS and APT can characterize microstructural features with varying sizes and morphologies and help identify at which point in material processing enrichment heterogeneities may have been introduced (if at all).

**Table 1.** Summary statistics for Student's t-tests for NanoSIMS and APT data collected for  $\gamma$ -UMo metal matrix and UC phases. The null hypothesis is that the population mean (of measured data) is equal to the test mean of 19.95 (i.e. the expected at. % <sup>235</sup>U). Data used in the statistical analysis is summarized in Figure 4. Confidence intervals (CI) were calculated at the 0.05 significance level.

	Population Mean	Standard Deviation	Degrees of Freedom	t-statistic	p-value	95% CI
NanoSIMS UMo	20.00	0.67	13	0.266	0.795	(19.61, 20.39)
APT UMo	19.76	0.41	8	-1.385	0.203	(19.45, 20.08)
NanoSIMS UC	19.65	0.58	13	-1.929	0.076	(19.32, 19.99)
APT UC	20.14	0.17	2	1.873	0.202	(19.71, 20.57)

## Conclusions

Our work highlights APT and NanoSIMS as complementary isotopic imaging modalities (that cover sub-nanometre to tens of micrometre length scales) capable of determining isotopic signatures with high accuracy and precision. These techniques can uncover material processing history or origin that is not possible with bulk techniques. In this study, the U enrichment measured by both NanoSIMS and APT is consistent with the expected, nominal isotopic composition of 19.95 at. % <sup>235</sup>U, indicating minimal residual HEU or DU feedstock materials were retained in the U-10Mo fuel samples.

## Conflicts of interest

There are no conflicts to declare.

## Acknowledgements

The current work was partly supported by the U.S. Department of Energy, National Nuclear Security Administration. The FIB-based sample preparation of LEU materials was conducted at the Radiochemical Processing Laboratory at the Pacific Northwest National Laboratory (PNNL). The APT and NanoSIMS analyses were performed using the facilities at the Environmental Molecular Sciences Laboratory, a national scientific user facility sponsored by the DOE's Office of Biological and Environmental Research and located at PNNL. PNNL is operated by the U.S. DOE under contract DE-AC05-76RL01830. The authors thank Dr. Douglas E. Burkes of PNNL for providing fuel samples for analysis. The authors also acknowledge Mr. Matthew Athon for providing a technical peer review of the manuscript.

## Author Contributions

E.J.K led manuscript writing with inputs from all co-authors. D.R. coordinated the metallographic preparation of samples used in this work. T.G.L., and D.R. performed site-specific sample preparation for NanoSIMS and APT analysis. T.G.L. and A.D. collected APT data. E.J.K, A.D, T.G.L. analysed APT data. J.C. collected and analysed all NanoSIMS data.

## Notes

Electronic supplementary information (ESI) available: Sample Preparation for NanoSIMS, Atom Probe Tomography Mass Spectra, Atom Probe Tomography Data Sets and Analysis. See DOI:

## References

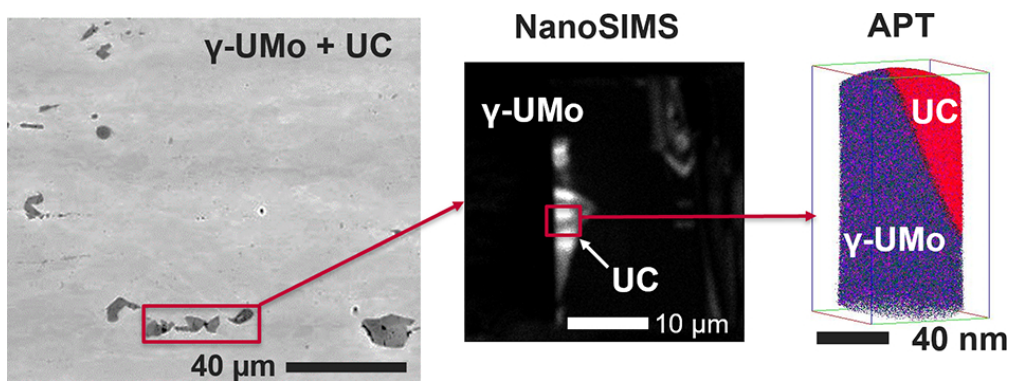
1. A. Devaraj, E. Kautz, L. Kovarik, S. Jana, N. Overman, C. Lavender and V. V. Joshi, *Scripta Materialia*, 2018, **156**, 70-74.
2. S. Jana, N. Overman, A. Devaraj, L. Sweet, C. Lavender and V. Joshi, *JOM*, 2019, **71**, 2770-2779.
3. E. J. Kautz, D. E. Burkes, V. V. Joshi, C. Lavendar and A. Devaraj, *Scientific Reports*, 2019.
4. A. J. Fahey, C. J. Zeissler, D. E. Newbury, J. Davis and R. M. Lindstrom, *Proceedings of the National Academy of Sciences*, 2010, **107**, 20207-20212.
5. R. Kips, P. K. Weber, M. J. Kristo, B. Jacobsen and E. C. Ramon, *Analytical Chemistry*, 2019, **91**, 11598-11605.
6. D. Reilly, M. Athon, L. Kovarik and T. Lach, *Materials Characterization*, 2019, **158**, 109948.
7. Z. Varga, M. Wallenius, A. Nicholl and K. Mayer, *Spectrochimica Acta Part B: Atomic Spectroscopy*, 2020, **171**, 105920.

## COMMUNICATION

## Journal Name

8. E. National Academies of Sciences, and Medicine., *Reducing the Use of Highly Enriched Uranium in Civilian Research Reactors*, The National Academies Press, Washington, DC, USA 2016.
9. J. Rest, Y. S. Kim, G. L. Hofman, M. K. Meyer and S. L. Hayes, *U-Mo fuels handbook. Version 1.0*, Argonne National Lab.(ANL), Argonne, IL (United States), 2006.
10. *HEU to LEU Conversion and Blending Facility: Metal Blending Alternative to Produce LEU Oxide for Disposal*, Nuclear Materials Disposition Program Office, Y-12 Plant Defense Programs, Y / ES-062 / R2, Oak Ridge, TN, 1995.
11. M. Meyer, J. Gan, J. F. Jue, D. Keiser, E. Perez, A. Robinson, D. Wachs, N. Woolstenhulme, G. Hofman and Y. S. Kim, *Irradiation performance of U-Mo monolithic fuel*, 2014.
12. S. Hu, D. E. Burkes, C. A. Lavender, D. J. Senior, W. Setyawan and Z. Xu, *Journal of Nuclear Materials*, 2016, **479**, 202 - 215.
13. M. J. Kristo, R. K. Bibby, A. M. Gaffney, V. G. Genetti, J. Go, J. M. Gostic, P. M. Grant, R. A. Henderson, I. D. Hutcheon, G. L. Klunder, K. B. Knight, C. Koester, R. E. Lindvall, A. N. Martin, K. J. Moody, C. E. Ramon, E. C. Ramon, M. Robel, M. A. Sharp, M. J. Singleton, P. E. Spackman, L. T. Summers, R. W. Williams and P. T. Woody, *Final Report - ITWG Round Robin #3*, United States, 2010.
14. L. Kovarik, A. Devaraj, C. Lavender and V. Joshi, *Journal of Nuclear Materials*, 2019, **519**, 287-291.
15. M. Bachhav, J. Gan, D. Keiser, J. Giglio, D. Jädernäs, A. Leenaers and S. Van den Berghe, *Journal of Nuclear Materials*, 2020, **528**, 151853.
16. S. S. Harilal, B. E. Brumfield, N. L. LaHaye, K. C. Hartig and M. C. Phillips, *Applied Physics Reviews*, 2018, **5**, 021301.
17. T. C. Kaspar, C. A. Lavender and M. W. Dibert, *Evaluation of Uranium-235 Measurement Techniques*, Report PNNL-26490, Pacific Northwest National Lab. (PNNL), Richland, WA (United States), 2017.
18. Y. Chen, Y. Shen, Z.-Y. Chang, Y.-G. Zhao, S.-L. Guo, J.-Y. Cui and Y. Liu, *Radiation Measurements*, 2013, **50**, 43-45.
19. C. Szakal, D. S. Simons, J. D. Fassett and A. J. Fahey, *Analyst*, 2019, **144**, 4219-4232.
20. J. S. Becker, *International Journal of Mass Spectrometry*, 2005, **242**, 183-195.
21. T. P. Forbes and C. Szakal, *Analyst*, 2019, **144**, 317-323.
22. B. T. Manard, C. Derrick Quarles, E. M. Wylie and N. Xu, *Journal of Analytical Atomic Spectrometry*, 2017, **32**, 1680-1687.
23. J. G. Tarolli, B. E. Naes, B. J. Garcia, A. E. Fischer and D. Willingham, *Journal of Analytical Atomic Spectrometry*, 2016, **31**, 1472-1479.
24. D. D. Reilly, C. L. Beck, E. C. Buck, J. B. Cliff, A. M. Duffin, T. G. Lach, M. Liezers, K. W. E. Springer, S. J. Tedrow and M. M. Zimmer, *Talanta*, 2020, **211**, 120720.
25. M. R. Kilburn and D. Wacey, 2014.
26. D. M. Perez, J. W. Nielsen, G. S. Chang and G. A. Ro, *AFIP-7 Irradiation Summary Report*, Idaho National Laboratory (INL), 2012.
27. G. A. Moore and M. C. Marshall, *AFIP-6 Fabrication Summary Report*.
28. R. Prabhakaran, V. V. Joshi, M. A. Rhodes, A. L. Schemer-Kohrn, A. D. Guzman and C. A. Lavender, *U-10Mo Sample Preparation and Examination using Optical and Scanning Electron Microscopy*, Report PNNL-25308, Pacific Northwest National Lab. (PNNL), Richland, WA (United States), 2016.
29. A. Devaraj, D. E. Perea, J. Liu, L. M. Gordon, T. J. Prosa, P. Parikh, D. R. Diercks, S. Meher, R. P. Kolli, Y. S. Meng and S. Thevuthasan, *International Materials Reviews*, 2018, **63**, 68–101.
30. K. Thompson, D. Lawrence, D. J. Larson, J. D. Olson, T. F. Kelly and B. Gorman, *Ultramicroscopy*, 2007, **107**, 131-139.
31. X. Hu, X. Wang, V. V. Joshi and C. A. Lavender, *Journal of Nuclear Materials*, 2018, **500**, 270-279.
32. F. Meisenkothen, M. McLean, I. Kalish, D. V. Samarov and E. B. Steel, *Analytical Chemistry*, 2020, DOI: 10.1021/acs.analchem.0c02273.

1  
2  
3  
4  
5  
6  
7  
8  
9  
10  
11  
12  
13  
14  
15  
16  
17  
18  
19  
20  
21  
22  
23  
24  
25  
26  
27  
28  
29  
30  
31  
32  
33  
34  
35  
36  
37  
38  
39  
40  
41  
42  
43  
44  
45  
46  
47  
48  
49  
50  
51  
52  
53  
54  
55  
56  
57  
58  
59  
60



80x29mm (300 x 300 DPI)